Inflammation Research (2025) 74:6
https://doi.org/10.1007/s00011-024-01973-7

Inflammation Research

ORIGINAL RESEARCH PAPER

Mitochondrial damage causes inflammation via cGAS-STING signaling in ketamine-induced cystitis

Jinji Chen[1] · Shengsheng Liang[1] · Cheng Li[1] · Bowen Li[1] · Mingdong He[1] · Kezhen Li[1] · Weijin Fu[1] · Shenghua Li[1] · Hua Mi[1]

Received: 11 August 2024 / Revised: 21 October 2024 / Accepted: 25 November 2024

Abstract

Background Mitochondrial dysfunction and damage can result in the release of mitochondrial DNA (mtDNA) into the cytoplasm, which subsequently activates the cGAS-STING pathway, promoting the onset of inflammatory diseases. Various factors, such as oxidative stress, viral infection, and drug toxicity, have been identified as inducers of mitochondrial damage. This study aims to investigate the role of mtDNA as a critical inflammatory mediator in the pathogenesis of ketamine (KET)-induced cystitis (KC) through the cGAS-STING pathway.

Methods To investigate the role of the cGAS-STING pathway in KET-induced cystitis, we assessed the expression of cGAS and STING in rats with KET cystitis. Additionally, we evaluated STING expression in conditionally deficient Simian Virus-transformed Human Uroepithelial Cell Line 1 (SV-HUC-1) cells in vitro. Morphological changes in mitochondria were examined using transmission electron microscopy. We measured intracellular reactive oxygen species (ROS) production through flow cytometry and immunofluorescence techniques. Furthermore, alterations in associated inflammatory factors and cytokines were quantified using real-time quantitative PCR with fluorescence detection.

Results We observed up-regulation of cGAS and STING expressions in the bladder tissue of rats in the KET group, stimulation with KET also led to increased cGAS and STING levels in SV-HUC-1 cells. Notably, the knockdown of STING inhibited the nuclear translocation of NF-κB p65 and IRF3, resulting in a decrease in the expression of inflammatory cytokines, including IL-6, IL-8, and CXCL10. Additionally, KET induced damage to the mitochondria of SV-HUC-1 cells, facilitating the release of mtDNA into the cytoplasm. This significant depletion of mtDNA inhibited the activation of cGAS-STING pathway, subsequently affecting the expression of NF-κB p65 and IRF3. Importantly, the reintroduction of mtDNA after STING knockdown partially restored the inflammatory response.

Conclusion Our findings confirmed the activation of the cGAS-STING pathway in KC rats and revealed mitochondrial damage in vitro. These results highlight the involvement of the cGAS-STING pathway in the pathogenesis of KC, suggesting its potential as a therapeutic target for intervention.

Keywords Mitochondrial damage · cGAS - STING signals · Ketamine-induced cystitis

Introduction

Ketamine(KET), a noncompetitive antagonist of the N-methyl-D-aspartate receptor, was first synthesized in the early 1960s and has since been employed for anesthesia and analgesia purposes [1, 2]. Additionally, KET modulates the function of glutamate receptors, particularly the NMDA receptor, within the neurotransmitter system, thereby eliciting an antidepressant effect [3, 4]. Due to its low cost, hallucinogenic properties, and potential for addiction, KET has increasingly emerged as a recreational drug, gaining popularity in regions such as Hong Kong, Taiwan, and

Communicated by John Di Battista.

✉ Hua Mi
mihua2019@163.com

[1] Department of Urology, The First Affiliated Hospital of Guangxi Medical University, Guangxi Zhuang Autonomous Region, Nanning, Guangxi, China

Published online: 07 January 2025

Europe [5, 6]. However, long-term abuse of KET not only induces acute toxic effects, such as hallucinations, perceptual changes, and distorted time perception, but also chronic toxic damage to the nervous system, cardiovascular system, and urinary system [7–9]. Urinary system damage resulting from ketamine abuse presents as lower urinary tract symptoms, including severe dysuria, hematuria, and urge urinary incontinence [10]. Cystoscopy reveals erythema, ulcers, and mucosal bleeding in the bladder, a condition known as KET-induced cystitis (KC) [11]. Various mechanisms have been implicated in the pathogenesis of KC, including direct stimulation of the bladder mucosa by KET and its metabolites, immune cell infiltration, and oxidative stress-induced damage [12]. The complexity of the KC's pathogenesis is evident, and the lack of effective treatment strategies remains a challenge. Therefore, it is essential to further investigate the pathogenesis of KC and explore novel treatment strategies.

Cyclic GMP-AMP synthase (cGAS) serves as an intracellular DNA sensor that primarily binds to DNA, initiating a cascade of reactions that includes the synthesis of cyclic guanosine monophosphate-adenosine monophosphate (cGAMP) [13]. cGAMP is a crucial signaling molecule that interacts with stimulator of interferon genes (STING), resulting in dimer formation. This interaction prompts STING to translocate from the endoplasmic reticulum (ER) to the ER-Golgi intermediate compartment and Golgi apparatus [14]. Upon dimerization with cGAMP, STING recruits and enhances the phosphorylation of tank-binding kinase 1 (TBK1) phosphorylation. Subsequently, phosphorylated TBK1 activates interferon regulatory factor 3 (IRF3) through phosphorylation [15]. This phosphorylation event is significant, as it activates IRF3 and collaborates with Nuclear Factor-kappa B (NF-κB) to induce the production of type I interferons [16]. This is the well-established GAS-STING signaling pathway functions not only as a host defense mechanism but also as a pivotal mediator of inflammation in various conditions, including infection, cellular stress, and tissue damage, thus playing a critical role in regulating the incidence and progression of numerous inflammatory diseases.

In ischemic myocardial infarction, characterized by myocardial cell death due to inadequate blood supply to the heart, cardiac macrophages detect cellular demise and rupture, initiating a harmful inflammatory response. Studies have demonstrated that inflammation production is associated with the activation of the cGAS-STING-IRF3 pathway. Interestingly, the loss of cGAS enhances the repair process by priming macrophages toward a reparative phenotype [17]. Activation of the cGAS-STING pathway in a mouse model of inflammatory lung injury has been shown to impede endothelial cell proliferation and exacerbate disease progression [18]. Additionally, during acute kidney injury, activation of the cGAS-STING pathway triggers the release of cytokines and chemokines, leading to immune cell activation [19]. Furthermore, studies indicate that upregulation of STING in traumatic brain injury can result in increased expression of inflammatory factors, thereby amplifying the extent of brain injury [20]. In systemic lupus erythematosus (SLE), a typical chronic systemic autoimmune disease, literature reports elevated serum cGAMP levels in approximately 15% of the 41 patients studied, suggesting the involvement of the cGAS pathway [21]. Collectively, these findings indicate a potential association between cGAS-STING pathway activation, aberrant immune system activation, and intensified inflammatory response.

Mitochondria play a crucial role in maintaining cellular metabolic homeostasis; however, they are highly susceptible to damage and dysfunction. Troglitazone, a drug previously used to treat type 2 diabetes but withdrawn from the market due to hepatotoxicity, has been shown to cause damage to mitochondrial DNA (mtDNA), induce mitochondrial permeability, and impaired ATP production [22]. This illustrates the toxic effects of the drug on mitochondrial function. Additionally, oxidative stress can further exacerbate mitochondrial damage. Following such damage, mtDNA is released into the cytoplasm, where it functions as a damp-associated molecular pattern (DAMP) [23]. Intracellular cGAS is capable of recognizing and binding to mtDNA. Once cGAS binds with mtDNA, the cGAS-STING signaling pathway is activated, leading to the initiation of downstream reactions [24]. Although numerous studies have confirmed the association between cGAS-STING and inflammatory diseases, it remains unclear whether this pathway is involved in regulating the occurrence and progression of KC.

In this study, we utilized a rat model induced by KET and cultured SV-HUC-1 cells exposed to KET to investigate the role of mitochondrial damage and the cGAS-STING signaling pathway in KC (Fig. 1). Our findings demonstrated that the knockdown of STING significantly reduced the expression of inflammatory factors. These results indicate that the STING molecule may represent a promising therapeutic target for KC.

Methods

Animals and drug administration

Twenty female Sprague-Dawley (SD) rats weighing 200–250 g were randomly divided into three different ketamine dosage groups (5, 25, and 50 mg/kg/day) and a control group, with five rats in each group. The rats received intraperitoneal injected with either saline or KET over a 12-week

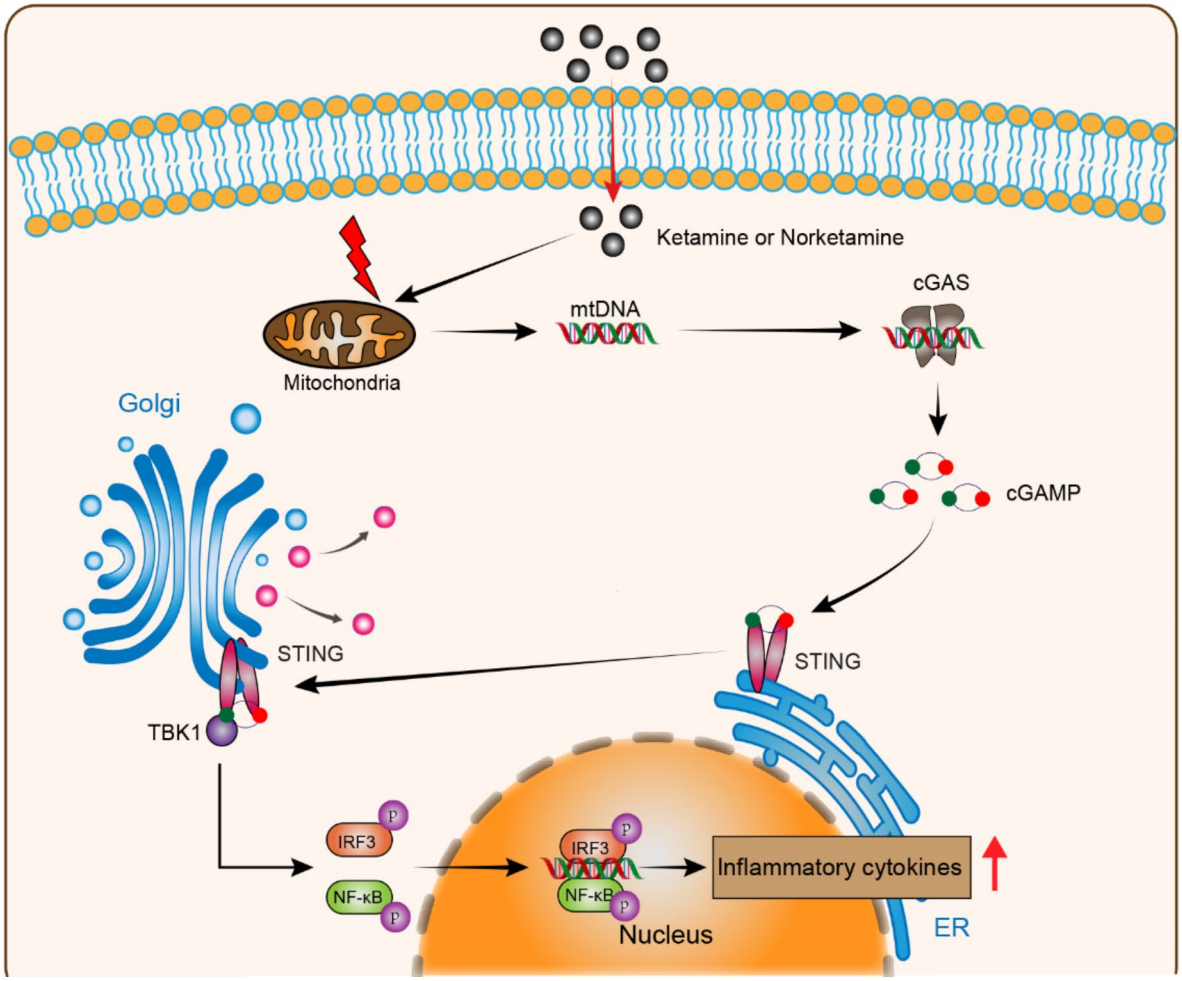

Fig. 1 KET disrupts mitochondrial function in SV-HUC-1 cells, leading to the release of mtDNA into the cytoplasm and activation of the cGAS-STING signaling pathway, thereby promoting the progression of KC

period. Weekly weight measurements were recorded, and the injection dosage was adjusted as needed to maintain consistent and adaptable dosing throughout the study. KET was produced by Jiangsu Hengrui Pharmaceutical Co., LTD. The drugs underwent rigorous quality control and testing to ensure purity and safety met the experimental requirements. The selected KET doses and administration durations were based on prior studies conducted in rats and mice [25–27]. All experimental procedures adhered to ethical requirements and received approval from the Ethics Committee of the First Affiliated Hospital of Guangxi Medical University.

Cell culture and treatment

The Simian Virus-transformed Human Uroepithelial Cell Line 1 (SV-HUC-1) cell line was purchased from the Cell Bank of the Chinese Academy of Sciences. SV-HUC-1 were incubated in accordance with the protocol as previously described [28]. Cells were cultured in Ham's F-12 K (Gibco, USA) medium supplemented with 10% fetal bovine serum (Sigma-Aldrich, China), and Penicillin-Streptomycin Liquid (Solarbio, Beijing, China) at 37 °C with 5% CO2. SV-HUC-1 cells were seeded in plastic tissue culture dishes with a diameter of 60 mm (Thermo Fisher Scientific), maintaining optimal growth conditions in the culture medium. Cells were stimulated with different concentrations of ketamine (1, 2, and 4 mmol/L) when the cell density in the culture dish reached approximately 80%. A control group was established by adding an equivalent volume of phosphate-buffered saline solution (PBS) to the medium. Control cells were incubated under the same conditions as the experimental group for 24 h but did not receive ketamine stimulation. Ethidium bromide (EtBr, Thermo Fisher Scientific) was utilized to deplete mtDNA and incubated with the cells for a duration of 48 h at a concentration of 1 μg/ml, following the described protocol [29].

RNA preparation and real-time PCR

Total RNA was extracted from SV-HUC-1 cells using an RNA extraction kit (Axygen, Hangzhou, China) following the manufacturer's instructions. The extracted total RNA served as a template for reverse transcription using PrimeScript RT Master Mix (Takara, Japan). To account for potential loss during repackaging, it is essential to ensure the accuracy of the reaction mixture volume, which should exceed one unit of the reaction system. Subsequently, add 3 μl of the mixed reaction liquid to each reaction tube, followed by the addition of enzyme-free water and the RNA samples under examination. Real-time PCR experiments were conducted using Fast Start Essential DNA Green Master (Roche, USA) on a real-time PCR instrument (LightCycler 96, Roche). The reaction conditions for the amplification process are as follows: First, the reaction undergoes predenaturation at 95 °C for 6 min. amplification process consists of three steps. Each cycle includes denaturation at 95 °C for 10 s, annealing at 60 °C for 10 s, and extension at 72 °C for 10 s. A total of 45 cycles are performed. Following the amplification cycles, the reaction is subjected to a melting step. During this step, the reaction is denatured at 95 °C for 10 s, annealed at 60 °C for 10 s, and extended at 72 °C for 10 s. Finally, the reaction is cooled down to 37 °C for 30 s. The relative gene expression levels were determined using the comparative cycle threshold (CT; 2^(-ΔΔCt)) method. Primer sequences are listed in KEY RESOURSE TABLE.

Western blotting

SV-HUC-1 cells and rat bladder tissue cells were lysed in RIPA buffer (Beyotime, P0013B) supplemented with a protein phosphatase inhibitor (Solarbio, Beijing, China) and centrifuged at 14,000 g for 10 min. Protein concentrations were quantified using the BCA method. Nuclear and Cytoplasmic Protein Extraction Kit (Beyotime, P0027) was used to extract nuclear and cytoplasmic proteins from SV-HUC-1 cells. Protein solutions were supplemented with a fivefold increase in protein loading buffer. The mixture is then heated at 100 °C for 10 min. The proteins were loaded onto SDS-PAGE gels and subjected to electrophoresis for protein separation. Subsequently, the proteins were transferred to PVDF membranes for immunoblot analysis. The membranes were subjected to blocking with 2.5% skim milk for 1 h at room temperature. Membranes were incubated with specific primary antibodies overnight at 4 ° C. The membranes were washed three times with TBST to remove nonspecifically bound antibodies, and then incubated with HRP-labeled secondary antibodies for 1 h at room temperature. After washing the membrane three times, develop it using an ECL chemiluminescence reagent kit. Quantitative analysis of the gray value of protein bands was performed using ImageJ software. All of the western blotting assays were performed and repeated 3 times. Information on primary and secondary antibodies is provided in KEY RESOURSE TABLE.

RNA interference

STING expression was suppressed with a siRNA against the human STING gene (Santa Cruz Biotechnology; sc-92042). Results were compared with a suppliermatched control siRNA (Santa Cruz Biotechnology; sc-37007). The siRNAs (10 nM) were introduced into SV-HUC-1 cells using Lipofectamine RNAiMAX transfection reagent (Thermo Fisher Scientific). After transfection (12–16 h), cells were stimulated as indicated.

Immunofluorescence (IF) staining

After the cultured cells were removed from the incubator, the old culture medium was discarded and the cells were washed with PBS. The SV-HUC-1 cells were fixed with 4% paraformaldehyde at room temperature for 20 min, followed by three washes with PBS. Cells were permeabilized with 0.1% Triton X-100 (Solarbio, Beijing, China) for 20 min, followed by blocking with 5% bovine serum albumin.

(BSA) for 30 min. The cells were incubated overnight at 4 °C with a primary antibody specific to dsDNA (1:300). Primary antibodies were diluted using an Immunol Staining Primary Antibody Dilution Buffer (Beyotime, P0103). Alexa Fluor 488 (Thermo Fisher Scientific, 1:300) was used as the secondary antibody. Then, cells were then incubated with 100nM MitoTracker Red CMXRos (Beyotime, C1035) in the medium for 20 min and washed twice with PBS. Detailed information regarding the antibodies used can be found in the KEY RESOURCE TABLE. The labeled cells were visualized using fluorescence microscopy (EVOS FL Tuto, AMAFD1000).

DNA isolation and mtDNA copy number analysis

Cytoplasm was extracted from SV-HUC-1 cells using a mitochondrial isolation kit (Beyotime, Beijing, China), and the resulting cytosolic supernatant, devoid of mitochondria, was collected. Subsequently, DNA was isolated from the collected cytoplasmic supernatants using a Genomic DNA minikit (Axygen, Hangzhou, China). Quantitative fluorescence PCR was conducted on a LightCycler 96 instrument using the Fast Start Essential DNA Green Master kit (Axygen, Hangzhou, China). mtDNA and nuclear DNA (nDNA) levels were determined by amplifying short regions of the trna-leuur and β2-microglobulin genes. The mRNA levels of the trna-leuur and β2-microglobulin genes were assessed

by QPCR, and the mtDNA copy number was assessed by calculating the ratio of the mRNA levels of the trna-leuur and β2-microglobulin genes (mtDNA/nDNA ratio) [30].

mtDNA isolation and transfection

mtDNA was successfully isolated from SV-HUC-1 cells using a mitochondrial DNA isolation kit (BioVision) [31]. The isolated mtDNA was suspended in TE buffer and stored at -20 ° C for future use. SV-HUC-1 cells were seeded in 6-well plates according to the manufacturer's instructions to culture and expand them for subsequent transfection experiments. mtDNA (1 μg per well, Thermo Fisher Scientific) was transfected into previously inoculated SV-HUC-1 cells using Lipofectamine 3000 (Thermo Fisher Scientific).

Measurement of mtROS

Mitochondrial reactive oxygen species (mtROS) levels in SV-HUC-1 cells were assessed by following the manufacturer's instructions for staining with MitoSOX Red dye (MCE; HY-D1055) [32]. SV-HUC-1 cells were treated with KET (2 mmol/L) for a duration of 24 h. Subsequently, the cells were stained with 5 μM MitoSOX Red dye for a duration of 10 min. Afterwards, the cells were washed with PBS to remove any unbound dye and fixed in paraformaldehyde for a duration of 10 min. Finally, the cells were counterstained with DAPI (Solarbio) for a duration of 10 min. The stained cells were visualized and captured using a Fluorescence microscope. ImagineJ software was used for quantitative analysis of fluorescence results.

Detection of ROS by flow cytometry

Detection of ROS using a Reactive Oxygen Species Assay Kit (Beyotime, S0033S) [33]. One million cells were added to 1 ml of PBS and thoroughly mixed. The mixture was then centrifuged at 1200 rpm for 5 min, and the supernatant was discarded. Following that, 2',7'-dichlorodihydrofluorescein diacetate (DCFH-DA) was diluted in serum-free culture medium at a 1:3000 ratio and thoroughly mixed. The diluted DCFH-DA solution was added to the cells, ensuring it adequately covered them. The cells were subsequently incubated at 37 °C in a light-protected environment for 30 min. After the incubation, the cells were washed three times with serum-free cell culture medium and then washed twice with PBS. The mixture was centrifuged at 1200 rpm for 5 min, and the supernatant was discarded. Finally, the cells were resuspended in 200 μl of PBS and subjected to analysis using the CytoFLEX S (BeckMen Coulter).

Immunohistochemistry (IHC) analysis

The tissue samples were initially fixed in 4% cold paraformaldehyde and subsequently embedded in paraffin blocks. Subsequently, deparaffinization, dehydration, antigen retrieval, and blocking procedures were conducted. Afterwards, the tissue sections were incubated with the respective antibodies overnight at 4 °C. The samples were incubated with HRP-labeled secondary antibodies for a duration of 30 min at 37 °C. Finally, tissue staining was conducted using diamino-benzidine H2O2 and hematoxylin. The tissue sections were immersed in a diaminobenzene-H2O2 solution and allowed to react for a specific duration to generate signals. Subsequently, the tissue sections were transferred to a heme solution for staining. Afterward, the tissue sections were washed to remove any excess stain. Finally, the tissue sections were observed and analyzed using a microscope. The histochemical images were converted to gray-scale images using Image J, and the average optical density values of the gray-scale images were measured. The difference of protein expression was compared by average optical density (AOD).

Statistical analysis

Statistical analysis was performed using GraphPad Prism 9, employing Student's t-tests or one-way analysis of variance (ANOVA) with a significance level set at $p < 0.05$. Multiple comparisons in one- or two-way ANOVA were corrected using the Sidak test. Data are presented as means ± standard deviations and represent a minimum of three independent experiments. ImagineJ software was utilized for quantifying the western blot results.

Results

Histological changes of bladder in KC rats

Histological examination through H&E staining results revealed that the bladder mucosa in the KET-treated group exhibited damage and disruption, with more pronounced submucosal congestion. These findings indicate that prolonged KET exposure adversely affects the bladder epithelium, resulting in inflammatory changes. Masson's trichrome staining was employed to visualize collagen fibers, which stained blue. Following ketamine treatment, an apparent increase in collagen fiber deposition was observed in both the submucosa and interstitium, in comparison to the control group. Notably, collagen deposition in in these regions intensified with higher concentrations of KET treatment (Fig. 2).

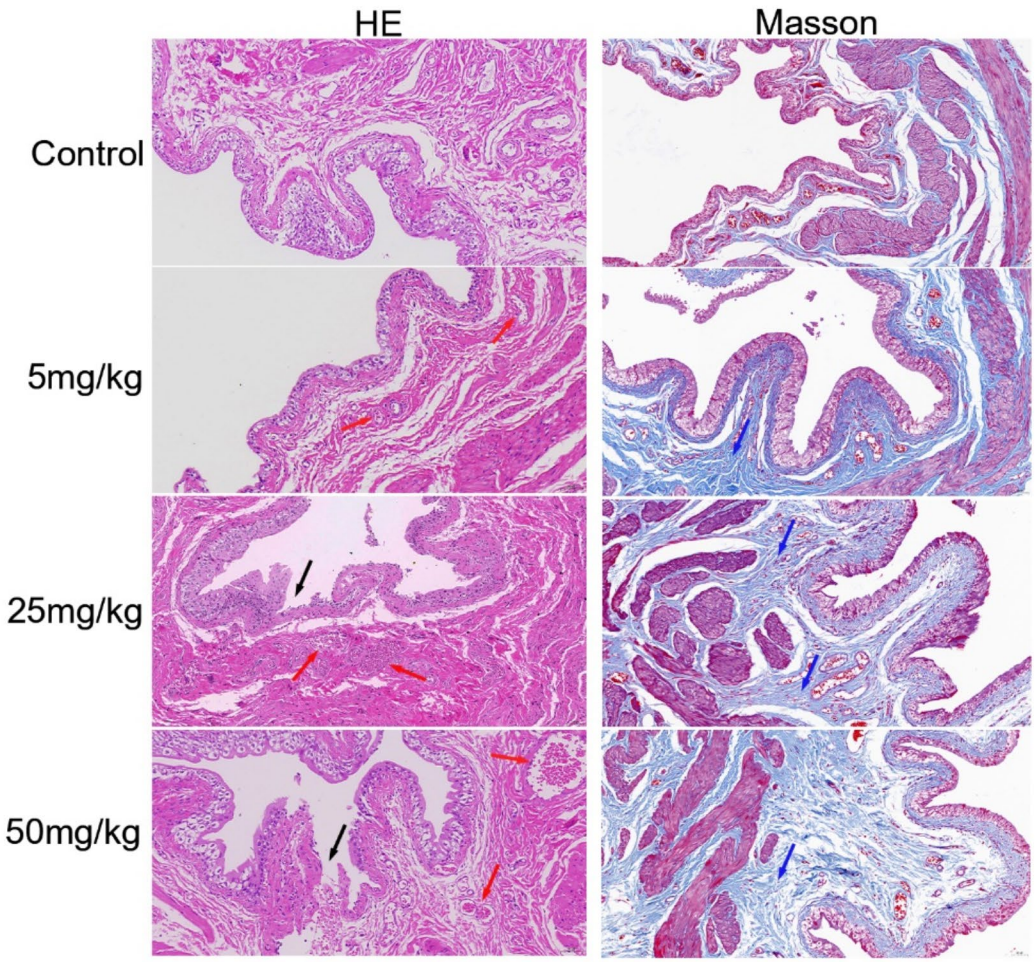

Fig. 2 HE staining and Masson staining were performed on the KC model group and the control group. (Red arrow: Submucosal congestion; Black arrows: mucosal damage and disruption; Blue arrow: collagen fiber deposition.)

The expression of cGAS and STING proteins were upregulated in the bladder tissue of rats in the KET-treated group

Immunohistochemical and Western blot analyses revealed a significant upregulation of cGAS and STING expression levels in the bladder tissue of the KET-treated group (Fig. 3B, C). These results collectively indicate the presence of inflammatory changes in the bladders of KET-treated rats, characterized by markedly elevated expression of cGAS and STING in the bladder tissue.

Ketamine activated the cGAS-STING pathway in SV-HUC-1 cells

To investigate the molecular mechanisms underlying bladder inflammation in a rat model of KC, the effect of the cGAS-STING pathway on SV-HUC-1cells were examined in vitro. Firstly, western blot analysis demonstrated a dose-dependent upregulation of cGAS and STING expression in SV-HUC-1 cells following KET exposure. Meanwhile, KET also increased the expression of phosphorylated TBK, a downstream molecule of cGAS-STING pathway (Fig. 4A). Additionally, real-time quantitative PCR analysis revealed that, compared to the control group, mRNA levels of downstream inflammatory-related factors, including IL-6, IL-8, CXCL10, IFN-α, and IFN-β, were significantly elevated in cells induced by KET via the cGAS-STING pathway (Fig. 4B). Collectively, these findings suggest that KET influences the cellular response by activating cGAS-STING signaling pathway.

cGAS-STING pathway activation increases KET-induced expression of inflammatory factors in SV-HUC-1 cells

To investigate the role of the cGAS-STING pathway on KC, STING knockdown assays were performed in bladder

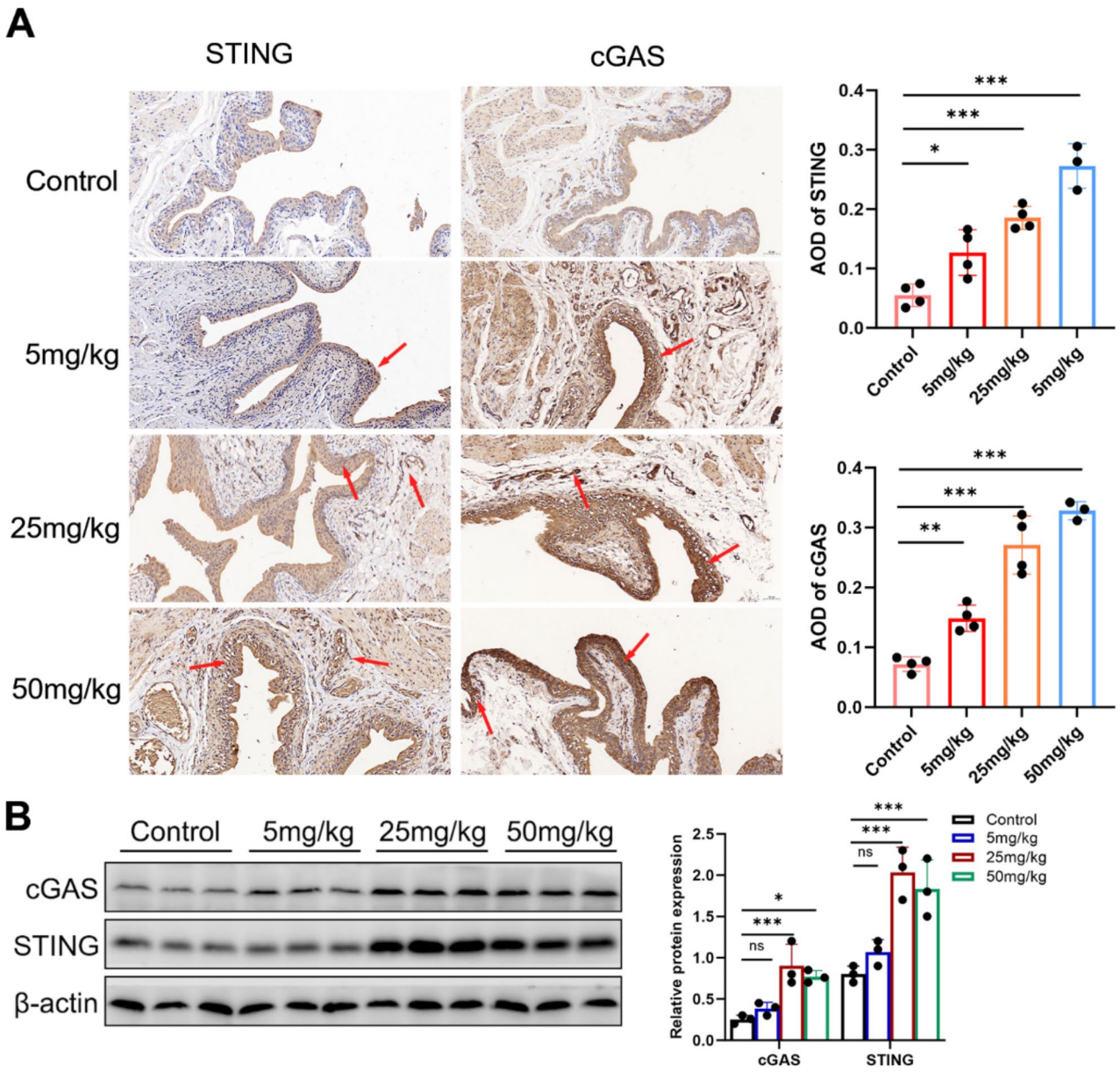

Fig. 3 KC in rats involves cGAS-STING signaling. **A** Immunohistochemical staining was employed to assess the expression levels of cGAS and STING in the bladder tissue samples obtained from both the control group and the ketamine group (Red arrow); AOD for cGAS and STING in the bladder tissues of both control and ketamine group of rats were determined ($n = 3$–4; $^{*}P < 0.05$, $^{***}P < 0.001$). **B** The protein expression of cGAS and STING in the bladder tissues of both ketamine and control group of rats was evaluated. ($n = 3$; $^{*}P < 0.05$, $^{***}P < 0.001$). Data were presented as mean ± SEM

epithelial cells. Western blot assay exhibited that STING knockdown significantly reduced the expression levels of phosphorylated TBK1 in SV-HUC-1 cells treated with KET (Fig. 5A). Furthermore, real-time quantitative PCR analysis showed that STING knockdown markedly reversed the KET-induced upregulation of inflammatory-related factors, including IL-6, IL-8, CXCL10, IFN-α, and IFN-β (Fig. 5B). This indicates that STING deficiency disrupts the regulation of inflammatory-related factors production and release.

Additionally, we assessed whether STING deficiency affected the expression and nuclear translocation of NF-κB p65 and IRF3 in vitro. Analysis of STING gene knockdown on the cytoplasmic and nuclear expression of NF-κB p65 and IRF3 in SV-HUC-1 cells demonstrated an increase in cytoplasmic levels of these proteins, while their levels in the nucleus decreased (Fig. 5C). This suggests that STING deficiency impairs the expression and nuclear translocation

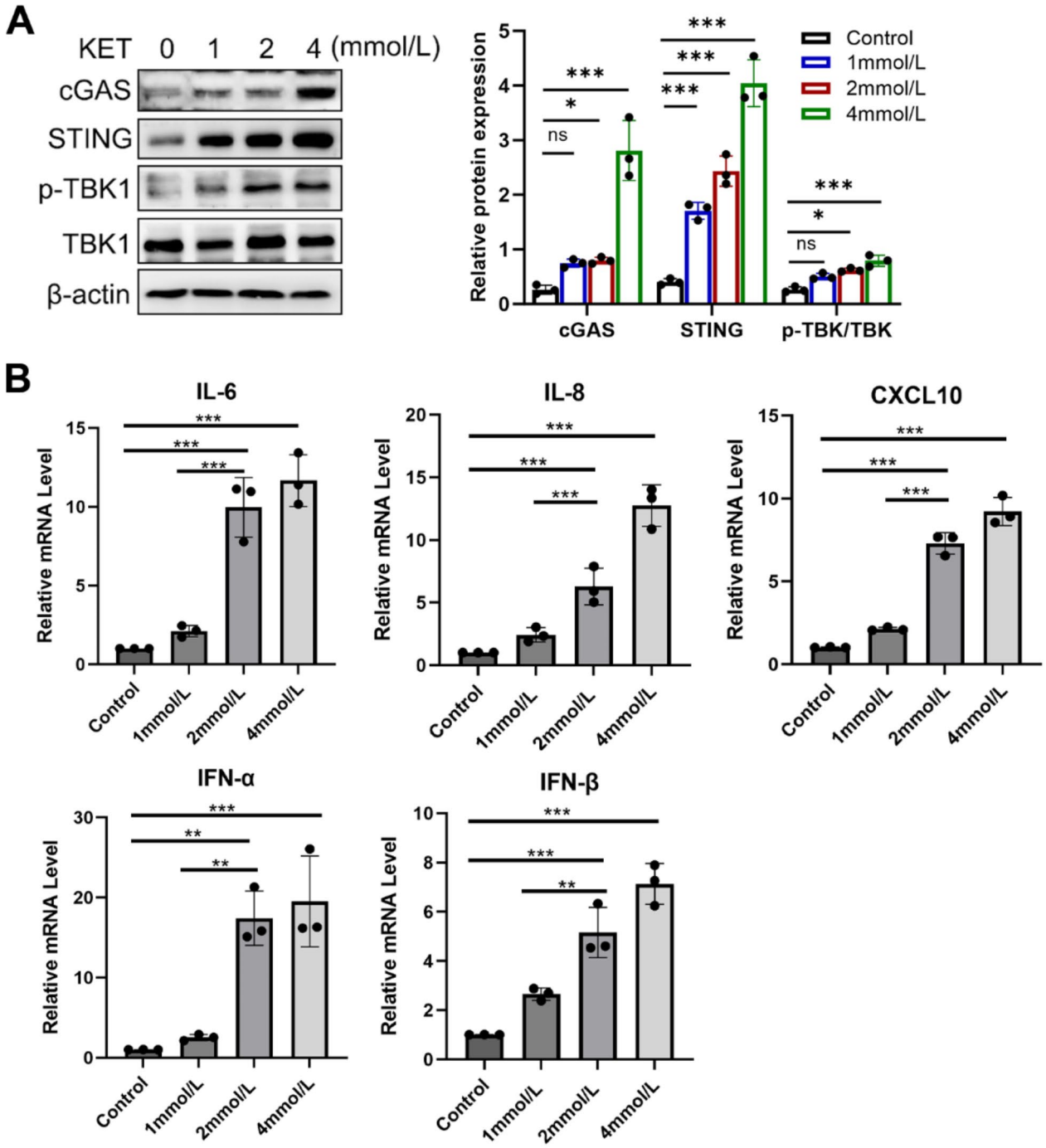

Fig. 4 Activation of the cGAS-STING pathway in SV-HUC-1 cells after KET stimulation. **A** Protein expression of cGAS and STING and phosphorylation of TBK1 in SV-HUC-1 cells ($n=3$; $^{*}P<0.05$, $^{***}P<0.001$). **B** mRNA expression levels of inflammatory cytokines in SV-HUC-1 cells treated with different concentrations of KET (1,2, and 4mmol/L) for 24 h ($n=3$; $^{*}P<0.05$, $^{**}P<0.01$, $^{***}P<0.001$). Data were presented as mean ± SEM

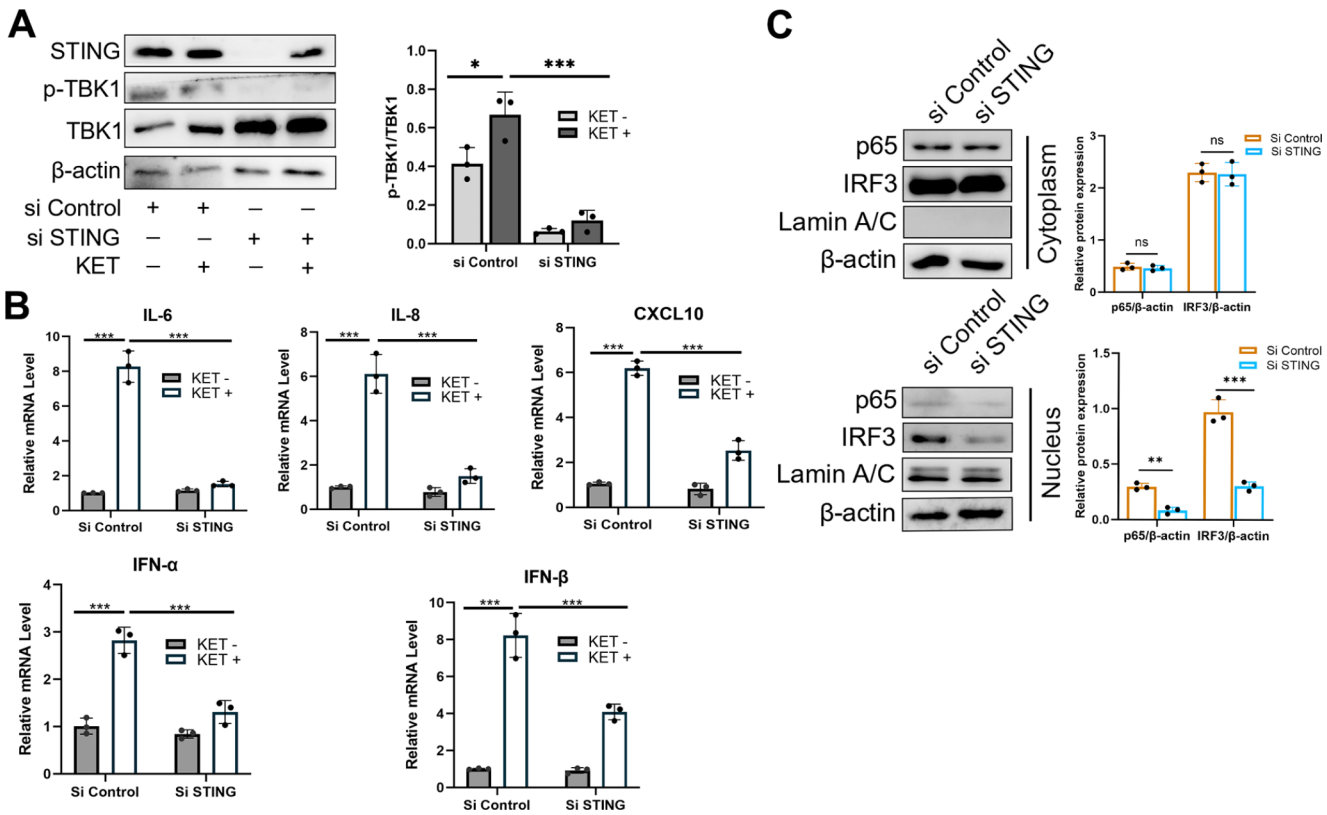

Fig. 5 The cGAS-STING pathway regulated KET-induced SV-HUC-1inflammation. **A** After a 24-hour ketamine stimulus (2 μM) on SV-HUC-1 cells with low STING expression, TBK and NF-κB p65 phosphorylation were observed ($n=3$; $^{*}P<0.05$, $^{***}P<0.001$) **B** The expression levels of proinflammatory factors and the mRNA of IFN-α and IFN-β were quantified using quantitative reverse transcription PCR in SV-HUC-1 cells with STING knockdown ($n=3$; $^{***}P<0.001$). **C** Western blot analysis was conducted to detect the expression of NF-κB p65 and IRF3 proteins in the cytoplasmic and nuclear fractions of SV-HUC-1 cells with STING knockdown ($n=3$; $^{**}P<0.01$, $^{***}P<0.001$). Data were presented as mean ± SEM

of NF-κB p65 and IRF3, potentially influencing the cellular inflammatory response and immune regulation.

KET induces mitochondrial damage and mtDNA leakage into the cytoplasm of SV-HUC-1 cells

We next investigated the causal relationship between KET and mitochondrial damage, specifically the leakage of mtDNA into the cytoplasm following such damage. The results from transmission electron microscopy (TEM) revealed that under KET stimulation, most cells exhibited mitochondrial shrinkage (Marked with red arrows) and condensation, accompanied by an increase in membrane density (Fig. 6A). Additionally, the expression of transcription factor A family protein (TFAM) was downregulated, while the expression of Bcl-2-associated X (BAX) protein was up-regulated in SV-HUC-1 cells following KET (2mmol/L, 24 h) stimulation, suggesting the occurrence of KET-induced mitochondrial damage (Fig. 6B). These findings provide evidence to support the assertion that KET induces mitochondrial damage in SV-HUC-1cells. Furthermore, the levels of superoxide anions were assessed using MitoSOX Red dye, and the results demonstrated that stimulation of SV-HUC-1 cells with KET (2mmol/L, 24 h) led to elevated generation of superoxide anions compared to the control group. (Fig. 5D). Flow cytometry analysis revealed that KET stimulation resulted in a significant increase in the production of intracellular ROS. Conversely, SV-HUC-1 cells with STING knockdown exhibited a notable reduction in ROS production, even under the same KET stimulation conditions (Fig. 5E). Furthermore, Double-stranded DNA (dsDNA) and mitochondrial double staining were performed on SV-HUC-1 cells. The results demonstrated that KET stimulation induced a significant increase in the cytoplasmic signal of dsDNA compared to the control, suggesting a pronounced translocation of dsDNA caused by KET (Fig. 5F). Real-time PCR results showed that KET stimulation increased mtDNA replication (Fig. 5G). Collectively, these findings strongly indicate that KET stimulation resulted in mitochondrial damage, leading to the generation of ROS and the release of mtDNA.

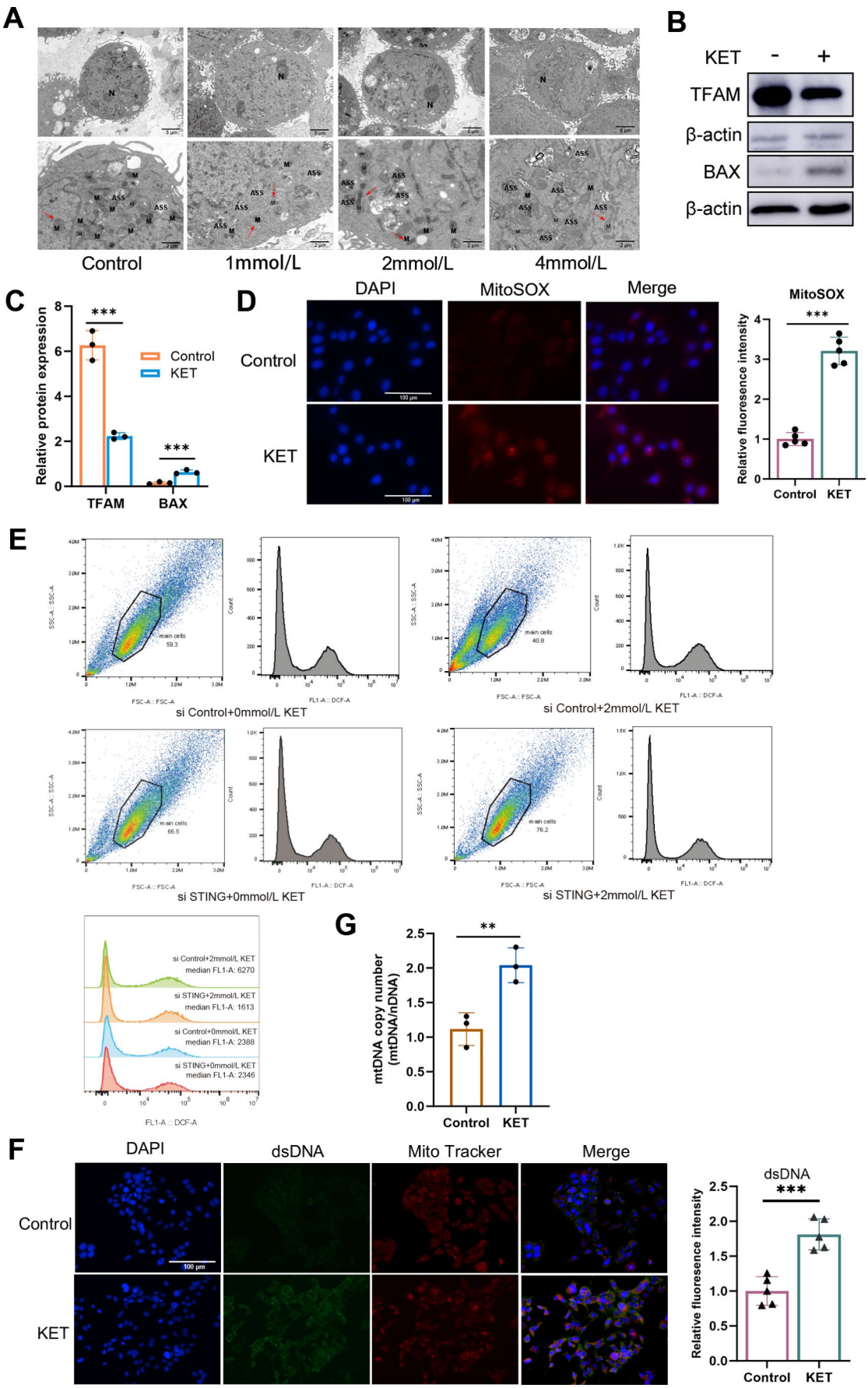
A
Control
1mmol/L
2mmol/L
4mmol/L
B
KET - +
TFAM
β-actin
BAX
β-actin
C
Relative protein expression
Control
KET
TFAM
BAX
D
DAPI
MitoSOX
Merge
Control
KET
MitoSOX
Relative fluorescence intensity
Control
KET
E
si Control+0mmol/L KET
si Control+2mmol/L KET
si STING+0mmol/L KET
si STING+2mmol/L KET
si Control+2mmol/L KET median FL1-A: 6270
si STING+2mmol/L KET median FL1-A: 1613
si Control+0mmol/L KET median FL1-A: 2388
si STING+0mmol/L KET median FL1-A: 2346
G
mtDNA copy number (mtDNA/nDNA)
Control
KET
F
DAPI
dsDNA
Mito Tracker
Merge
Control
KET
dsDNA
Relative fluorescence intensity
Control
KET

Fig. 6 KET induced mitochondrial injury and mtDNA leakage into the cytosol in SV-HUC-1cells. **A** Morphological changes of mitochondria in SV-HUC-1 cells were observed using TEM after stimulation with different concentrations of KET (1, 2, 4 mmol/L). scale bars, 5 μm and 2 μm ($n=3$). M: Mitochondria; ASS: Autolysosomes; N: Nuclei. **B** The protein expression of BAX and TFAM was evaluated in SV-HUC-1 cells following stimulation with KET (2 mmol/L, 24 h). **C** Quantification of TFAM and BAX protein expression ($n=3$; $^{***}P<0.001$). **D** MitoSOX Red staining was performed after stimulating SV-HUC-1 cells with KET (2mmol/L, 24 h). scale bars, 50 μm. The boxplot displays the signal intensity ($n=5$; $^{***}P<0.001$). **E** Flow cytometry was employed to measure the levels of ROS ($n=3$). **F** Double immunofluorescence staining of dsDNA and mitochondria was performed in SV-HUC-1 cells stimulated with KET (2 mmol/L,24 h). scale bars, 50 μm. The boxplot displays the signal intensity ($n=5$; $^{***}P<0.001$). **G** The copy number of mtDNA in SV-HUC-1 cells was determined using real-time quantitative PCR after ketamine stimulus ($n=3$; $^{**}P<0.01$). Data were presented as mean ± SEM

mtDNA leakage into the cytoplasm activates cGAS-STING signaling pathway KET-induced expression of inflammatory factors in SV-HUC-1 cells

To investigate the role of cytosolic mtDNA as a crucial trigger in the cGAS-STING pathway, we employed EtBr treatment to deplete mtDNA from SV-HUC-1 cells. The results revealed that EtBr treatment led to an approximately 80% reduction in mtDNA copy number in SV-HUC-1 cells (Fig. 7A). KET stimulation inhibited TBK1 phosphorylation in cells depleted of mtDNA (Fig. 7B), while the expression of inflammatory cytokines IL-6, IL-8, and CXCL10 is significantly reduced (Fig. 7C). To confirm the role of mtDNA in the nuclear translocation of NF-κB p65 and IRF3, we analyzed the protein expression of NF-κB p65 and IRF3 in the nucleus and cytoplasm of EtBr-treated SV-HUC-1 cells. Following EtBr treatment, the results revealed alterations in the protein levels of NF-κB p65 and IRF3. Specifically, cytoplasmic levels increased while nuclear levels decreased (Fig. 7D). This indicates that the absence of mtDNA hinders the nuclear translocation of NF-κB p65 and IRF3, thereby impacting their functionality within the nucleus. Subsequently, we performed transfection of isolated mtDNA into SV-HUC-1 cells. Notably, the introduction of mtDNA into the cytoplasm triggered the phosphorylation of TBK-1 (Fig. 7E). Additionally, this mtDNA transfection led to the upregulation of downstream inflammatory factors (Fig. 7F). In summary, our findings clearly demonstrate that in the inflammatory response of SV-HUC-1 cells, leaked mtDNA in the cytoplasm plays a crucial role through the cGAS-STING pathway.

Discussion

KET is utilized in medicine as both an anesthetic and for the treatment of depression. However, over the last 15 years, KET abuse has emerged as a significant global issue, particularly among adolescents. KET abuse is a prevalent, with approximately one-third of long-term abusers experiencing urinary system symptoms [34, 35]. Histological analysis of bladder tissue samples from patients with KC reveals urothelial mucosal exfoliation, ulceration, collagen deposition, smooth muscle degeneration, vascular proliferation, eosinophil infiltration, and elevated levels of several inflammatory marker [36]. The intricate pathogenesis of KC presents a formidable challenge for effective treatment [37]. In recent years, substantial research has been dedicated to investigating the cGAS-STING pathway and its association with inflammatory diseases [38–40]. Additionally, interventions aimed at modulating this pathway have been explored to regulate the development of inflammation and slow disease progression.

Several potential mechanisms have been proposed to elucidate the relationship between mitochondrial damage and the release of mtDNA [41]. Mitochondria, as the primary site of ROS generation, are susceptible to various cellular components, including proteins, lipids, and DNA damage. Furthermore, mitochondria are themselves vulnerable to ROS-induced damage [42, 43]. These ROS can harm mitochondrial membranes and DNA, further compromising their structure and function. Previous studies have indicated a relationship between inflammation in KC and oxidative stress mediated by mitochondria and the endoplasmic reticulum [44]. mtDNA exhibits higher susceptibility to oxidative damage compared to nuclear DNA. This increased vulnerability can be attributed to the proximity of mtDNA to the respiratory chain within the inner mitochondrial membrane, the absence of protective histone-like proteins, and its limited capacity for damage repair [45]. Damage to mtDNA can affect the stability of the sufficient ATP supply to the cell and disrupt the balance of apoptosis, mitochondrial bioenergetics, and biogenesis [46]. Our results demonstrate that ketamine induces a significant increase in mtROS production in SV-HUC-1 cells, reflecting a close association between ketamine-induced inflammation and oxidative stress.

The integrity of both the inner and outer mitochondrial membranes is crucial for maintaining mtDNA within the mitochondria [47]. Prior research has indicated that the elevation of mitochondrial outer membrane permeability through BAX activation triggers alterations in inner membrane permeability, ultimately leading to the release of mitochondrial matrix constituents, including mtDNA [48]. Additionally, TFAM forms a tightly bound association with

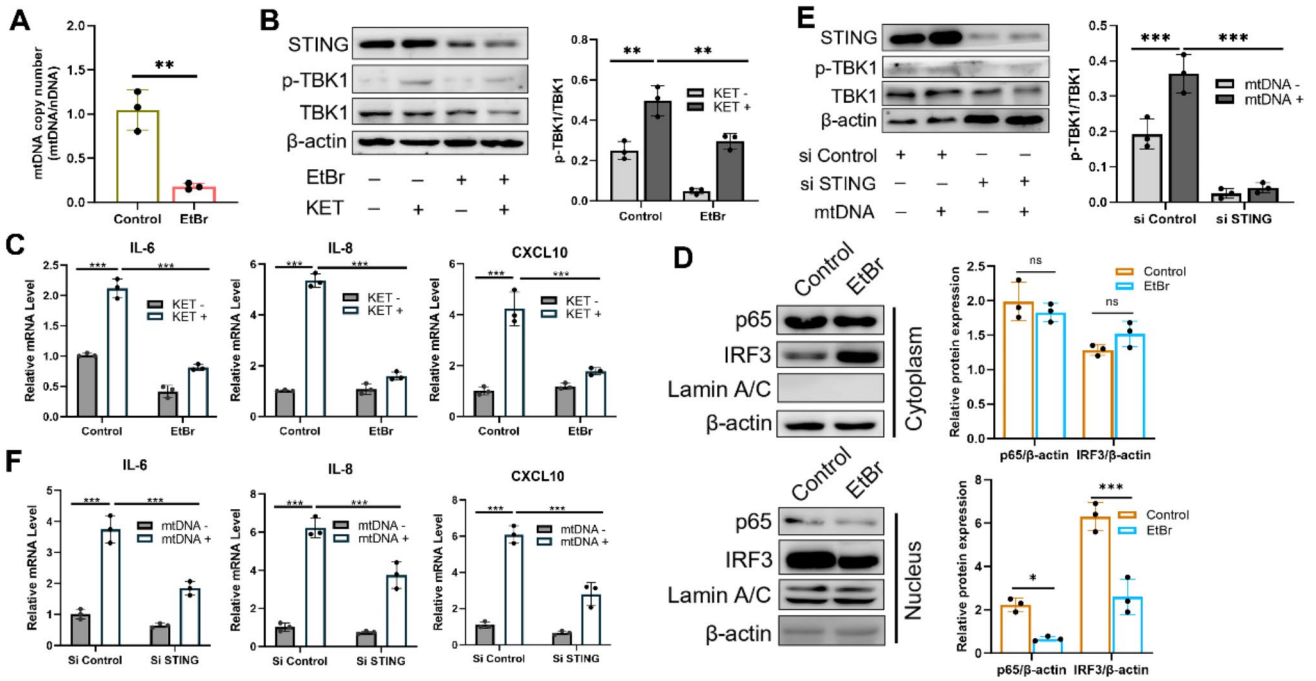

Fig. 7 mtDNA leakage into the cytosol activated the cGAS-STING pathway in SV-HUC-1 cells co-cultured with KET. **A** SV-HUC-1 cells were treated with EtBr, and quantitative PCR was conducted to measure the copy number of mtDNA ($n=3$; $^{**}P<0.01$). **B** Following the treatment of cells with EtBr, the level of TBK1 phosphorylation was assessed. The data were represented quantitatively, including the relative ratio to the total level of TBK1($n=3$; $^{**}P<0.01$). **C** The mRNA levels of inflammatory factors in SV-HUC-1 cells were measured using real-time PCR following treatment with EtBr ($n=3$; $^{***}P<0.001$). **D** The cytoplasmic and nuclear protein levels of NF-κB p65 and IRF3 were assessed in SV-HUC-1 cells after treatment with EtBr ($n=3$; $^{*}P<0.05$, $^{***}P<0.001$). **E** Transfection of mtDNA in STING-knockdown cells resulted in changes in the level of TBK1 phosphorylation. The quantitative data represents the relative proportion to the total level of TBK1($n=3$; $^{***}P<0.001$). **F** The mRNA levels of inflammatory factors were measured after transfection of mtDNA in STING-knockdown cells. Data are expressed as mean ± SEM

the mitochondria, enveloping mtDNA and contributing to its stability and integrity [49]. Consequently, the loss or dysfunction of TFAM may increase the instability of mtDNA, rendering it more vulnerable to oxidative damage [50]. BAX, a member of the BCL-2 family, is essential for inducing apoptosis and increasing mitochondrial outer membrane permeability (MOM) [51]. It can modulate the dynamics of apoptotic pore expansion and consequently facilitate the release of mtDNA [52]. In SV-HUC-1 cells stimulated with ketamine, the protein level of BAX was found to be elevated, while the protein level of TFAM was decreased. These findings suggest that ketamine treatment of cells may reduce the stabilizing effect of TFAM on mtDNA, resulting in increased permeability of mitochondrial membranes and easier release of mitochondrial DNA into the cytoplasm. Observations from TEM revealed notable changes in SV-HUC-1 cells in the ketamine group, including reduced cellular volume, nuclear fragmentation, increased heterochromatin density, significant shrinkage of mitochondria, increased membrane density with high electron density, altered crista structures, and an increase in autophagolysosomes. Collectively, these observations indicate mitochondrial damage.

Numerous studies have substantiated that the overactivation of the STING signaling pathway can trigger aberrant inflammatory responses and autoimmune diseases [53, 54]. Exposing SV-HUC-1 cells to ketamine resulted in the upregulation of inflammatory factors, including IL-6, IL-8, and CXCL10. Conversely, upon STING knockdown in SV-HUC-1 cells, the expression of inflammatory factors diminished, and the phosphorylation of downstream targets, namely TBK1 and NF-κB p65, was impeded. Prior studies have demonstrated the involvement of the NF-κB pathway in the pathogenesis of ketamine-associated cystitis [28]. Thorough investigation of the STING signaling pathway will enhance our understanding of inflammatory regulatory mechanisms and offer novel strategies and targets for the treatment of associated diseases.

The leakage of mtDNA from impaired mitochondria is regarded as a significant contributor to inflammatory activation, thereby influencing the pathogenesis of various inflammation-related disorders [19]. Notably, exposure of SV-HUC-1 cells to KET resulted in observable mitochondrial damage, concomitantly leading to the leakage of mtDNA into the cytoplasm and subsequent activation of the STING pathway. EtBr treatment inhibited the

phosphorylation of TBK1 in SV-HUC-1 cells, as well as the nuclear translocation of NF-κB p65 and IRF3, resulting in reduced expression of inflammatory factors IL-6, IL-8, and CXCL10. These findings imply that depleting mtDNA can suppress the inflammatory response. However, transfection of mtDNA into STING knockdown SV-HUC-1 cells partially reinstated the expression of inflammatory factors. These findings underscore the crucial involvement of the cGAS-STING pathway in the genesis of inflammation in KC, with mtDNA emerging as a particularly critical initiator of the cGAS-STING pathway.

Our study has several limitations. Although the bladder tissue of KC rats in our model showed changes in cGAS and STING proteins, further research utilizing STING knockout animals or specific STING inhibitors is needed to explore the pathological role of the cGAS-STING pathway in KC more comprehensively. Additionally, we did not exclude the potential involvement of other DNA sensors in the activation of mtDNA. Therefore, future studies should focus on further validation and refinement of these findings.

This study aimed to investigate the role of the cGAS-STING signaling pathway in KC. Notably, previous research has established a regulatory relationship between cGAS-STING and the NLRP3 signaling pathway. For instance, in human embryonic kidney (HEK293T) cells infected with herpes simplex virus type 1 (HSV-1), STING recruits NLRP3 and facilitates its localization to the endoplasmic reticulum, thereby promoting inflammasome formation [55]. In human myeloid cells, STING is involved in cytosolic DNA induced-NLRP3 inflammasome activation [56]. Additionally, KET has been shown to promote apoptosis and induce inflammatory responses both in vitro and in vivo by regulating the NLRP3/TXNIP axis [57]. In the context of KC, it is possible that cGAS-STING may exacerbate inflammatory progression through its regulation of NLRP3, a hypothesis that warrants further investigation. Moreover, NLRP3 has been implicated in the progression of cyclophosphamide-induced interstitial cystitis and diabetic bladder dysfunction [58, 59]. The potential association of cGAS-STING signaling with these conditions, and whether it mediates the onset of cystitis or bladder dysfunction through the regulation of NLRP3, remains to be explored further.

In summary, our findings elucidate the crucial role of mtDNA leakage induced by mitochondrial damage in the inflammation of SV-HUC-1 cells following KET exposure. This event subsequently triggers activation of the cGAS-STING signaling pathway, leading to inflammatory responses. Moreover, we observed increased expression of cGAS-STING signaling pathway-related proteins in a rat model of KC. Therefore, therapeutic interventions aimed at targeting STING may provide promising anti-inflammatory strategies for managing KC.

Supplementary Information The online version contains supplementary material available at https://doi.org/10.1007/s00011-024-01973-7.

Author contributions JJC, SSL, and HM designed experiments. JJC drafted the manuscript. SSL, CL, BWL, MDH, WJF, SHL, and KZL participated in revision of manuscript for important intellectual content. JJC, SSL, CL, and BWL performed the experiments. JJC, SSL, CL, and BWL take responsibility for the accuracy of the analysis of the whole experiment. All authors read and approved the final manuscript. JJC SSL, and CL contributed equally to this work.

Funding This study was supported by the National Natural Science-Foundation of China (81860142).

Data availability No datasets were generated or analysed during the current study.

Declarations

Competing interests The authors declare no competing interests.

References

1. Aroni F, Iacovidou N, Dontas I, et al. Pharmacological aspects and potential new clinical applications of ketamine: reevaluation of an old drug. J Clin Pharmacol. 2009;49(8):957–64.
2. Zanos P, Moaddel R, Morris PJ, et al. Ketamine and ketamine metabolite pharmacology: insights into therapeutic mechanisms. Pharmacol Rev. 2018;70(3):621–60.
3. Smith-Apeldoorn SY, Veraart JK, Spijker J, et al. Maintenance ketamine treatment for depression: a systematic review of efficacy, safety, and tolerability. Lancet Psychiatry. 2022;9(11):907–21.
4. Murrough JW. Ketamine as a novel antidepressant: from synapse to behavior. Clin Pharmacol Ther. 2012;91(2):303–9.
5. Xu J, Lei H. Ketamine-an update on its clinical uses and abuses. CNS Neurosci Ther. 2014;20(12):1015–20.
6. Yang HH, Jhang JF, Hsu YH, et al. Smaller bladder capacity and stronger bladder contractility in patients with ketamine cystitis are associated with elevated TRPV1 and TRPV4. Sci Rep. 2021;11(1):5200.

7. Parkin MC, Turfus SC, Smith NW, et al. Detection of ketamine and its metabolites in urine by Ultra high pressure liquid chromatography-tandem mass spectrometry. J Chromatogr B Analyt Technol Biomed Life Sci. 2008;876(1):137–42.
8. Bokor G, Anderson PD. Ketamine: an update on its abuse. J Pharm Pract. 2014;27(6):582–6.
9. Lee YL, Lin KL, Chuang SM, et al. Elucidating mechanisms of bladder repair after hyaluronan instillation in ketamine-induced ulcerative cystitis in animal model. Am J Pathol. 2017;187(9):1945–59.
10. Pal R, Balt S, Erowid E et al. Ketamine is associated with lower urinary tract signs and symptoms. Drug and Alcohol Dependence, 2013, 132(1–2): 189– 94.
11. Shahani R, Streutker C, Dickson B, et al. Ketamine-associated ulcerative cystitis: a new clinical entity. Urology. 2007;69(5):810–2.
12. Baker SC, Shabir S, Georgopoulos NT, et al. Ketamine-Induced apoptosis in normal human urothelial cells: a direct, N-Methyl-d-aspartate receptor-independent pathway characterized by mitochondrial stress. Am J Pathol. 2016;186(5):1267–77.
13. Chen C, Xu P. Cellular functions of cGAS-STING signaling. Trends Cell Biol. 2023;33(8):630–48.
14. Ishikawa H, Ma Z, Barber GN. Sting regulates intracellular DNA-mediated, type I interferon-dependent innate immunity. Nature. 2009;461(7265):788–92.
15. Gui X, Yang H, Li T, et al. Autophagy induction via STING trafficking is a primordial function of the cGAS pathway. Nature. 2019;567(7747):262–6.
16. Chen Q, Sun L, Chen ZJ. Regulation and function of the cGAS-STING pathway of cytosolic DNA sensing. Nat Immunol. 2016;17(10):1142–9.
17. Cao DJ, Schiattarella GG, Villalobos E, et al. Cytosolic DNA sensing promotes macrophage transformation and governs myocardial ischemic injury. Circulation. 2018;137(24):2613–34.
18. Huang LS, Hong Z, Wu W, et al. mtDNA activates cGAS signaling and suppresses the YAP-mediated endothelial cell proliferation program to promote inflammatory injury. Immunity. 2020;52(3):475–86. e5.
19. Chung KW, Dhillon P, Huang S et al. Mitochondrial damage and activation of the sting pathway lead to renal inflammation and fibrosis. Cell Metab, 2019, 30(4): 784– 99 e5.
20. Witcher KG, Eiferman DS, Godbout JP. Priming the inflammatory pump of the CNS after traumatic brain injury. Trends Neurosci. 2015;38(10):609–20.
21. An J, Durcan L, Karr RM, et al. Expression of cyclic GMP-AMP synthase in patients with systemic lupus erythematosus. Arthritis Rheumatol. 2017;69(4):800–7.
22. Rachek LI, Yuzefovych LV, Ledoux SP, et al. Troglitazone, but not rosiglitazone, damages mitochondrial DNA and induces mitochondrial dysfunction and cell death in human hepatocytes. Toxicol Appl Pharmacol. 2009;240(3):348–54.
23. Wallace DC. Mitochondrial genetic medicine. Nat Genet. 2018;50(12):1642–9.
24. Aarreberg LD, Esser-Nobis K, Driscoll C et al. Interleukin-1beta induces mtDNA release to activate Innate Immune Signaling via cGAS-STING. Mol Cell, 2019, 74(4): 801– 15 e6.
25. Wu P, Shan Z, Wang Q, et al. Involvement of mitochondrial pathway of apoptosis in urothelium in ketamine-associated urinary dysfunction. Am J Med Sci. 2015;349(4):344–51.
26. Shen CH, Wang ST, Wang SC, et al. Ketamine–induced bladder dysfunction is associated with extracellular matrix accumulation and impairment of calcium signaling in a mouse model. Mol Med Rep. 2019;19(4):2716–28.
27. Zhu Q, Li K, Li H, et al. Ketamine induced bladder fibrosis through MTDH/P38 MAPK/EMT pathway. Front Pharmacol. 2021;12:743682.
28. Xi XJ, Zeng JJ, Lu Y, et al. Extracellular vesicles enhance oxidative stress through P38/NF-kB pathway in ketamine-induced ulcerative cystitis. J Cell Mol Med. 2020;24(13):7609–24.
29. Hashiguchi K, Zhang-Akiyama Q-M. Establishment of human cell lines lacking mitochondrial DNA. Mitochondrial DNA. 2009: 383– 91.
30. Maekawa H, Inoue T, Jao T-M et al. Mitochondrial damage causes inflammation via cGAS-STING signaling in acute kidney injury. SSRN Electron J, 2019.
31. Zhou L, zhang Y-F, Yang F-H et al. Mitochondrial DNA leakage induces odontoblast inflammation via the cGAS-STING pathway. Cell Commun Signal, 2021, 19(1).
32. Price OT, Lau C, Zucker RM. Quantitative fluorescence of 5-FU–treated fetal rat limbs using confocal laser scanning microscopy and Lysotracker Red. Cytometry Part A. 2003;53A(1):9–21.
33. Esteban MA, Wang T, Qin B, et al. Vitamin C enhances the generation of mouse and human induced pluripotent stem cells. Cell Stem Cell. 2010;6(1):71–9.
34. Sassano-Higgins S, Baron D, Juarez G, et al. A review of ketamine abuse and diversion. Depress Anxiety. 2016;33(8):718–27.
35. Kalsi SS, Wood DM, Dargan PI. The epidemiology and patterns of acute and chronic toxicity associated with recreational ketamine use. Emerg Health Threats J. 2011;4:7107.
36. Lin HC, Lee HS, Chiueh TS, et al. Histopathological assessment of inflammation and expression of inflammatory markers in patients with ketamine-induced cystitis. Mol Med Rep. 2015;11(4):2421–8.
37. Jhang JF, Hsu YH, Kuo HC. Possible pathophysiology of ketamine-related cystitis and associated treatment strategies. Int J Urol. 2015;22(9):816–25.
38. Ouyang W, Wang S, Yan D, et al. The cGAS-STING pathway-dependent sensing of mitochondrial DNA mediates ocular surface inflammation. Signal Transduct Target Ther. 2023;8(1):371.
39. Gulen MF, Samson N, Keller A, et al. cGAS-STING drives ageing-related inflammation and neurodegeneration. Nature. 2023;620(7973):374–80.
40. Zou M, Ke Q, Nie Q, et al. Inhibition of cGAS-STING by JQ1 alleviates oxidative stress-induced retina inflammation and degeneration. Cell Death Differ. 2022;29(9):1816–33.
41. Zhong Z, Liang S, Sanchez-Lopez E, et al. New mitochondrial DNA synthesis enables NLRP3 inflammasome activation. Nature. 2018;560(7717):198–203.
42. Williams RS. Canaries in the coal mine: mitochondrial DNA and vascular injury from reactive oxygen species. Circ Res. 2000;86(9):915–6.
43. Ide T, Tsutsui H, Hayashidani S, et al. Mitochondrial DNA damage and dysfunction associated with oxidative stress in failing hearts after myocardial infarction. Circ Res. 2001;88(5):529–35.
44. Liu KM, Chuang SM, Long CY, et al. Ketamine-induced ulcerative cystitis and bladder apoptosis involve oxidative stress mediated by mitochondria and the endoplasmic reticulum. Am J Physiol Ren Physiol. 2015;309(4):F318–31.
45. Clayton DA. Transcription of the mammalian mitochondrial genome. Annu Rev Biochem. 1984;53:573–94.
46. Quan Y, Xin Y, Tian G et al. Mitochondrial ROS-Modulated mtDNA: a potential target for cardiac aging. Oxid Med Cell Longev, 2020, 2020: 9423593.
47. Chan DC. Mitochondrial dynamics and its involvement in disease. Annu Rev Pathol. 2020;15:235–59.
48. Mcarthur K, Whitehead LW, Heddleston JM, et al. BAK/BAX macropores facilitate mitochondrial herniation and mtDNA efflux during apoptosis. Science. 2018;359(6378):eaao6047.
49. Kang D, Kim SH, Hamasaki N. Mitochondrial transcription factor A (TFAM): roles in maintenance of mtDNA and cellular functions. Mitochondrion. 2007;7(1–2):39–44.

50. Zhao M, Wang Y, Li L, et al. Mitochondrial ROS promote mitochondrial dysfunction and inflammation in ischemic acute kidney injury by disrupting TFAM-mediated mtDNA maintenance. Theranostics. 2021;11(4):1845–63.
51. Czabotar PE, Lessene G, Strasser A, et al. Control of apoptosis by the BCL-2 protein family: implications for physiology and therapy. Nat Rev Mol Cell Biol. 2014;15(1):49–63.
52. Cosentino K, Hertlein V, Jenner A, et al. The interplay between BAX and BAK tunes apoptotic pore growth to control mitochondrial-DNA-mediated inflammation. Mol Cell. 2022;82(5):933–e499.
53. Zhou L, Zhang YF, Yang FH, et al. Mitochondrial DNA leakage induces odontoblast inflammation via the cGAS-STING pathway. Cell Commun Signal. 2021;19(1):58.
54. Hu Y, Chen B, Yang F, et al. Emerging role of the cGAS-STING signaling pathway in autoimmune diseases: biologic function, mechanisms and clinical prospection. Autoimmun Rev. 2022;21(9):103155.
55. Wang W, Hu D, Wu C, et al. STING promotes NLRP3 localization in ER and facilitates NLRP3 deubiquitination to activate the inflammasome upon HSV-1 infection. PLoS Pathog. 2020;16(3):e1008335.
56. Gaidt MM, Ebert TS, Chauhan D, et al. The DNA inflammasome in human myeloid cells is initiated by a sting-cell death program upstream of NLRP3. Cell. 2017;171(5):1110–e2418.
57. Cui L, Jiang X, Zhang C et al. Ketamine induces endoplasmic reticulum stress in rats and SV-HUC-1 human uroepithelial cells by activating NLRP3/TXNIP aix. Biosci Rep, 2019, 39(10).
58. Kiran S, Rakib A, Singh UP. The NLRP3 inflammasome inhibitor dapansutrile attenuates cyclophosphamide-induced interstitial cystitis. Front Immunol. 2022;13:903834.
59. Hughes FM, Allkanjari JR, Odom A. Diabetic bladder dysfunction progresses from an overactive to an underactive phenotype in a type-1 diabetic mouse model (Akita female mouse) and is dependent on NLRP3. Life Sci. 2022;299:120528.